Chemically Exfoliated Titanium Carbide *MXene* for Highly Sensitive Electrochemical Sensors for Detection of 4-Nitrophenols in Drinking Water

Rajavel Krishnamoorthy, Karuppasamy Muthumalai, Thiba Nagaraja, Ramasamy Thangavelu Rajendrakumar, and Suprem R Das*

Read Online

ACCESS | Metrics & More | Article Recommendations | Supporting Information

ABSTRACT: Soil and water contamination by numerous pollutants has been increasingly posing threats to food, water, agriculture, and human health. Using novel nanoscale materials to develop rapid electrochemical sensors is very promising due to the discovery of a number of new two-dimensional (2D) electronic materials. Of particular importance is 2D transition-metal carbide *MXene* that has been shown to possess transformative properties pertaining to its physical, chemical, and environmental characteristics, leading to their potential sensor applications. Designing electrochemical sensors using *MXene* has the potential to pave the way for monitoring environmental pollutants. Here, a stacked layer of chemically exfoliated *MXene* ($Ti_3C_2T_x$) was demonstrated as an electrochemical sensor for detection of 4-nitrophenol (4-NP) with high sensitivity and a low limit of detection. Successful selective exfoliation of the MAX (Ti_3AlC_2) phase of the material by chemical etching without oxidation is shown to be the key to achieving higher sensitivity and a lower detection limit. In the optimal conditions, the proposed *MXene* sensor electrodes were capable of detecting 4-NP in a broad concentration range from 500 nM to 100 μM with a good linear sensing range (regression fit, R = 0.995). The higher sensitivity and notable limit of detection reached about 16.35 μA μM^{-1} cm^{-2} and 42 nM/L, respectively, with good reproducibility and repeatability. The real-time application of the proposed *MXene* sensor electrodes was confirmed by testing in tap water samples with excellent recoveries of 95−99%.

1. INTRODUCTION

Soil and water constitute important components in food, water, agriculture, environment, and global climate sustainability.[1,2] Furthermore, water and soil purity have a direct impact on human health and plant growth. On the other hand, excessive human activities such as industrialization, urbanization, and modern farming with overuse of fertilizers and pesticides are causing numerous pollutions in the soil and water networks and posing a serious threat to our ecosystem. Therefore, monitoring contaminants in water and soil is one of the urgent needs. However, the lack of precision sensors to detect contaminants in water and soil hinders such efforts. Aromatic chemical compounds anchored with nitrogen groups are widely used in petroleum industries, pharmaceuticals, pesticides, dyes, and other chemical factories. Generally, aromatic molecules containing nitrogen derivatives are more carcinogenic to ecosystems, including both nonliving and living systems. Among specific interests in the nitrated phenol family, such as 2-nitrophenol (2-NP), 3-nitrophenol (3-NP), and 4-nitrophenol (4-NP), the latter one has been identified as the most serious toxic phenolic derivative.[3−5] 4-NP has critical effects on the growth and metabolism of living organisms, including humans, specifically causing methemoglobinemia, liver and kidney injuries.[6−8] Because of its continuous exposure, causing drowsiness, cyanosis, lethargy, and nausea,

the environmental protection agency (EPA) categorizes the limit of 4-NP in drinking water to be less than 0.43 μM.[5−7,9] Therefore, the development of rapid, continuous, selective, and trace-level detection of 4-NP from all sources especially water is required. At present, many approaches including traditional methods such as spectroscopy, fluorimetry, electrophoresis, high-performance liquid chromatography (HPLC), chemiluminescence, competitive flow assays, and electrochemical methods have been applied for qualitative and quantitative identification of pollutants specifically 4-NP.[2,7,8] Among the different analytical methods, electrochemical techniques are of current interest because of its rapid response, cost-effectiveness, simple operation, and importantly, its potential in realtime and in-field monitoring. However, fundamental to this method lies its first validation of analyte sensitivity, selectivity, stability (reliability), and low detection limits metrics, which are still in a developmental stage.[5,6] Recently, 2D *MXene* has

been benchmarked as an excellent material among other low dimensional systems to fabricate reliable electrochemical sensors.[10]

Furthermore, *MXene* materials have gone through significant advancements in bioapplication areas such as electrochemical sensors, biofuel cell design, environmental remediation, bioimaging, biosensor, photothermal therapy, drug delivery, theranostics, antibacterials, and cytocompatibility.[10−13] *MXenes* ($M_{n+1}X_nT_x$, with $n = 1−3$, where M is the transition metal, X is either carbon or nitrogen, and T_x stands for adsorbed species on the surface such as −OH and −F) are primarily prepared by removing the metal layer from their host ternary ceramic MAX by chemical etching, where M is the transition metal, A is either a group IIA or IVA element, and X can be either carbon and/or nitrogen atoms.[14−18] 2D *MXene* material is of interest owing to its versatile physicochemical properties, comprehensive excellent metallic conductivity originating from abundant electron densities at the Fermi level, great hydrophilicity, and easy solution processability.[10,19,20] In addition to that, during the chemical exfoliation process, the attachment of functional (−OH, −F, and =O) moieties on *MXene* has its own active performance, which anchors other functional groups.[21,22] The outstanding conductivity of *MXene* has been identified as a promising substrate of choice when it comes to developing electrochemical sensing technology and is expected to have better performance compared with other 2D layered nanostructures.[10] Titanium carbide ($Ti_3C_2T_x$) is the first reported and widely studied candidate among the *MXene* family and could be used for different electrochemical sensor fabrications such as glucose, environmental pesticide, and pharmaceutical compound detection.[23,24] Additionally, among the *MXene* family with different compositions, the first explored *MXene*-$Ti_3C_2T_x$ shows high metallic conductivities (6000−8000 S/cm)[25,26] compared with other 2D layered materials that possess promising applications. Their excellent intrinsic electrical conductivity in combination with their reactive hydrophilic surface renders them active materials in electrochemical sensor applications.[27] For environmental phenolic-based pollutant detection using *MXene* in electrochemical analysis, Wu et al. reported that the stacked $Ti_3C_2T_x$ combined with tyrosinase (enzyme) immobilization can detect the phenol molecules; however, in their work, the analysis of selectivity performance is not well carried out. The sensitivity is also lower, which may not be very effective for trace-level detection of 4-nitrophenol (4-NP) in water.[28] Recently, nanoparticle-embedded *MXene* materials have been used to enhance the sensitivity of electrochemical sensors. For example, an electrostatically attached Zn-Co-N doped carbon nanocage with Nb_2CT_x showed remarkable electrochemical detection of 4-NP.[29,30] In another study, enhanced electrocatalytic performance toward bisphenol A was demonstrated by anchoring Pt nanoparticles with a Nafion binder on Ti_3C_2.[31] The development of electrochemical sensors for the detection of 4-NP with affordable sensitivity using bare stacked *MXene* nanostructures by understanding the material quality is still an active area of research. Recently, hydrothermally assisted exfoliated multilayer oxidized $Ti_3C_2T_x$ *MXene* for simultaneous detection of 4-chlorophenol and 4-nitrophenol in water samples has been reported with a lower sensitivity and detection limit.[32] To the best of our knowledge, the fabrication of unique 4-NP electrochemical sensor electrodes using stacked $Ti_3C_2T_x$ layers by a controlled exfoliation process that possess excellent sensitivity, selectivity, limit of detection

and with different pH environments and a similar homologous structure to 4-NP has not been established.

In this present study, we emphasize on the importance of controlled exfoliated $Ti_3C_2T_x$-*MXene* without any external surface treatment to enrich the electrochemical and catalytic properties leading to high sensitivity and the low detection limit of 4-NP. Optimally controlled chemical etching conditions form bulk stacked 2D *MXene* ($Ti_3C_2T_x$) with functional moieties that are the key parameters for successful *MXene*-based electrochemical 4-NP sensors. Our *MXene* on glassy carbon electrode (GCE) electrochemical sensors showed excellent electrochemical performance and catalytic reduction of 4-NP with high sensitivity (16.35 μA μM^{-1} cm^{-2}), a detection range of 500 nM to 100 μM, and reproducibility alongside a good linear detection and low detection limit (42 nM/L) even in the occurrence of similar intrusive nitrogen aromatic groups. A reliable performance tested toward 4-NP diagnosis in real complex tap water using our sensors could be applied in future environmental pollutant monitoring applications.

2. RESULTS AND DISCUSSION

2.1. Synthesis of 2D *MXene*. The following results of structural and morphological characterization evidenced that formation of *MXene* stacked layers is obtained from a ceramic MAX phase: the exfoliated *MXene* layered structure was observed using SEM and TEM and results are shown in Figure 1a−f. Figure 1a−d shows the SEM images with a gradual
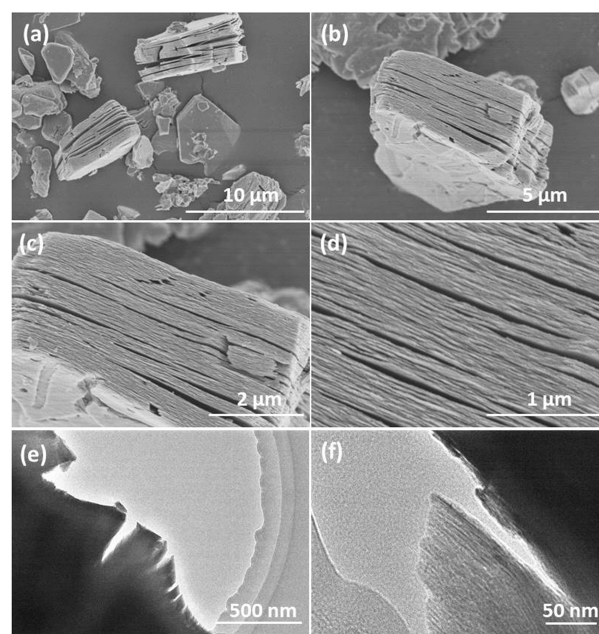
Figure 1. (a−d) SEM visualization of the chemically exfoliated *MXene* nanostructures under different magnifications and (e, f) TEM characterization of compact stacked *MXene* layers.

increase in magnification, where a micrometer scale thickness of the plates is visible along with the layered structure within the plates' cross section. The compact structure of the MAX phase material is shown in the Figure S1a,b, and after the chemical etching of the Al layers in MAX phase, the material was converted into 2D *MXene* and reassembled into a stacked and highly packed 2D accordion-like structure (Figure 1a−d). Although these are thick platelet types of structure (TEM
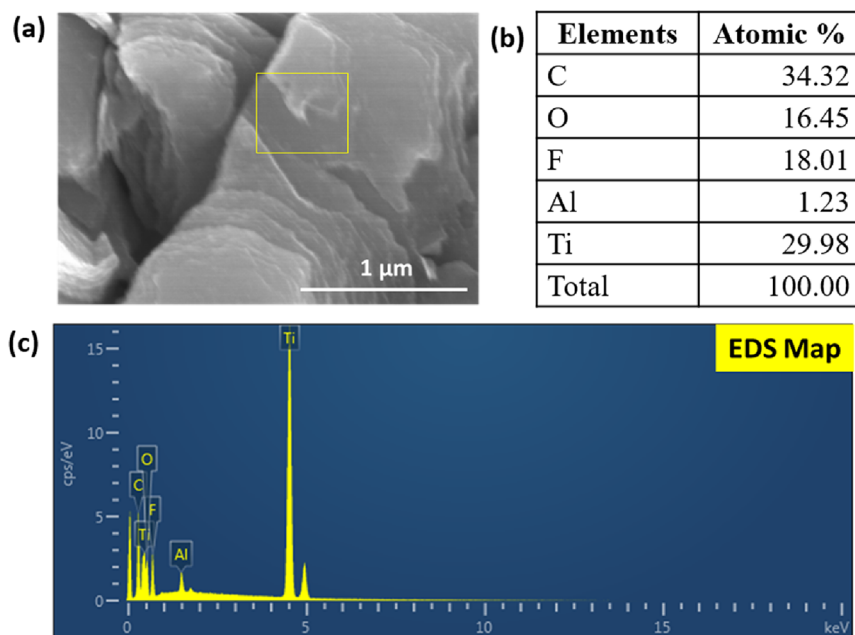
Figure 2. EDS elemental analysis of *MXene* extracted from MAX after chemical exfoliation.
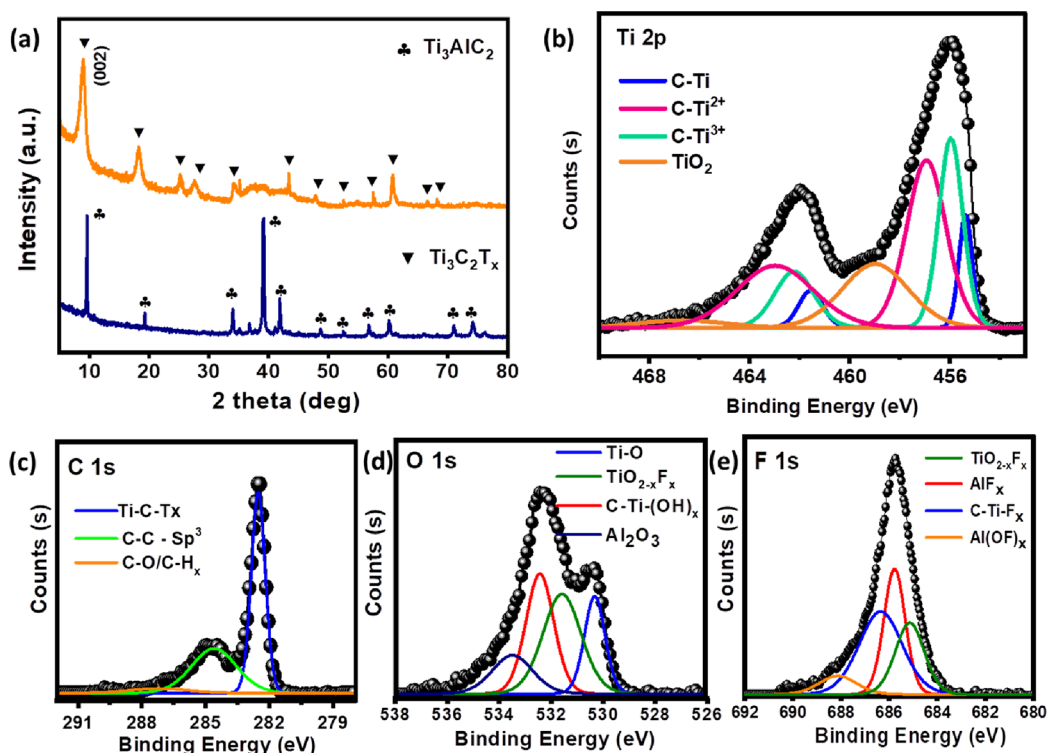
Figure 3. (a) X-ray diffraction spectra of MAX and chemically exfoliated *MXene*, (b−e) XPS deconvoluted spectra of *MXene* and its individual elemental (Ti 2p, C 1s, and O 1s) deconvoluted peak fittings.

image shown in Figure 1e), these nanoscale edges are exposed for interactions with the environment (line structures shown in the TEM image, Figure 1f). Further, the HR-TEM image shows (Figure S2) stacking of individual *MXene* layers with measured d spacing of about 0.817 ± 0.14 nm.[33] The EDS elemental analysis of the stacked layers after chemical etching, shown in Figure 2, largely demonstrates the presence of both elemental Ti and C and the measured elemental ratio of each component is given in Figure 2b. However, the small Al

content indicates residual aluminum that is reduced substantially after repeated washing cycles. The oxygen and fluorine signature comes from $Ti_3C_2T_x$, where T_x represents −OH and −F functional groups.[25] In addition, the FTIR spectrum of exfoliated *MXene* in transmittance mode after mixing with KBr powder was collected and the results are presented in Figure S3. The vibrational band observed at 606 cm^{-1} represents out of plane vibrations of Ti−C. The band positions noted at 1385 and 3504 cm^{-1} correspond to stretching vibrational modes of
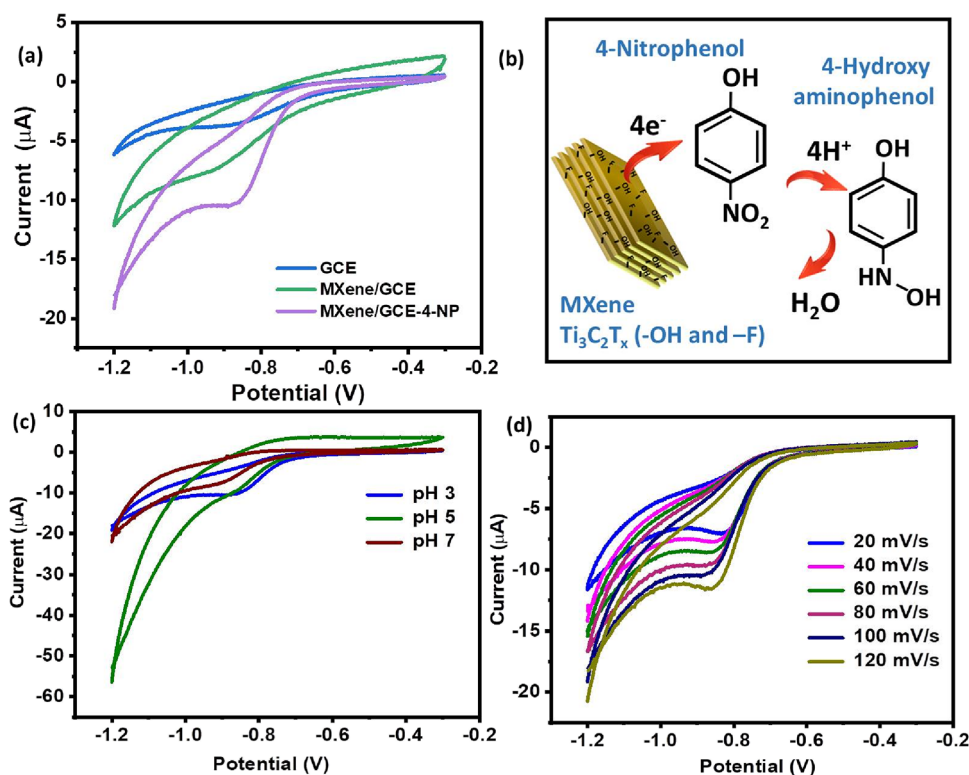
Figure 4. (a) CV graphs of bare and *MXene*-modified GCE electrodes measured in 100 mV/s (0.1 M PBS and pH 3) with and without 4-NP (100 μM) addition, (b) schematic illustration about electrochemical reduction of 4-NP in the presence of the *MXene*, (c) CV curves of *MXene*/GCE tested in different pH conditions, and (d) CV curves of *MXene*/GCE immersed in 0.1 M PBS (pH 3) with 100 μM 4-NP under different scan rate in the range between −20 to 120 mV/s,

−OH groups associated with Ti⁴⁺.[34] The bands observed at 462 and 649 cm⁻¹ indicate Ti−O from hydroxyl functional groups and oxide nanoparticles.[35] The exfoliated *MXene* contains adsorbed water molecules and C−F, supporting the spectrum bands at 1641 and 1076 cm⁻¹, respectively.[36] As we will discuss later, the oxygen in the hydroxyl group is not detrimental for sensing. However, it is very important to rule out any formation of quality *MXene* with primary elements Ti and C. Practices to develop controlled exfoliation processes for the synthesis of a stacked *MXene* structure without the aid of a longer post-sonication process and etching chemicals could enrich charge transport properties and ultimately lead to superior performance of devices such as sensors.[25,37] The crystalline features of the MAX phase of the material before and after chemical etching were analyzed using X-ray diffraction (XRD) measurements, and the results are presented in Figure 3a. The vanishing of the dominant MAX phase peak around $2\theta \approx 37.9°$ and shifting of peak at $2\theta \approx 9.65°$ in the MAX phase to a lower angle confirm the formation of 2D *MXene*.[38,39] The calculated interlayer d spacing (9.89 Å) and lattice parameter (19.53 Å) at the lower angle peak position of *MXene* (002) are consistent with previous reports indicating the successful exfoliation of *MXene* layers.[37] Other diffraction peaks at $2\theta \approx 9.03°$, 18.19°, 25.20°, 27.62°, 34.19°, 43.51°, 47.87°, 52.57°, 57.47°, 60.93°, 66.62°, and 68.31° correspond to the bulk stacked *MXene*.[20,40] The lower angle shifting of the (002) peak from $2\theta \approx 9.65°$ to 8.94° further confirms the exfoliated *MXene* material with an expanded interlayer distance (from 9.10 to 9.89 Å).[20,38]

The X-ray photoelectron spectroscopy (XPS) analysis of chemically treated MAX-phase ceramic materials, as described

above, was performed to evaluate the chemical environment of the constituent atoms (such as titanium, carbon, oxygen, fluorine) and presence of adsorption species (such as −F, −OH, =O, etc.). XPS measurements were made using the monochromatic Al Kα (1486.6 eV) radiation mentioned above. Figure S4 shows the full XPS survey of the synthesized *MXene* with C 1s, Ti 2p, O 1s, and F 1s with their relative energy values in the binding energy spectrum. The XPS full survey spectrum confirms the removal of the intermediate Al layer and the assembly of a *MXene* layered structure. The individual elemental peaks along with their deconvoluted peaks originating from the presence of underlying chemical species are shown in Figure 3b−e. The Ti 2p spectrum has two peaks around 456 and 462 eV, corresponding to Ti 2p$_{3/2}$ and Ti 2p$_{1/2}$, respectively, due to spin-orbit splitting. After deconvolution, the peak split for Ti 2p$_{3/2}$ was observed at 455.37, 455.96, 457.24, and 458.98 eV corresponding to C−Ti, C−Ti²⁺, C−Ti³⁺, and TiO₂, respectively. Similarly, for Ti 2p$_{1/2}$, the de-convoluted spectrum split into 461.16, 461.82, 462.98, and 464.79 eV corresponding to C-Ti, C-Ti²⁺, C-Ti³⁺, and TiO₂, indicating successful exfoliation of *MXene*.[38,41,42] For the C 1s spectra (Figure 3c), the deconvoluted peaks were fitted at 282.51, 284.60, and 287.21 eV, corresponding to C−Ti−T$_x$ (moiety I, II, III, or IV), C−C, and CH$_x$/C−O, respectively, confirmed the attachment of surface functional groups such as −OH, −O, and −F on the surface and edges of stacked layered assembly during Al removal and washing cycles.[41] In the case of the O 1s region, as presented in Figure 3d, the XPS peaks are fitted at 529.82, 530.86, 531.86, and 532.75 eV relating to Ti−O, C−Ti−O$_x$, Al₂O₃, and the adsorption of water, respectively.[38,41] The O 1s deconvoluted spectra demonstrate
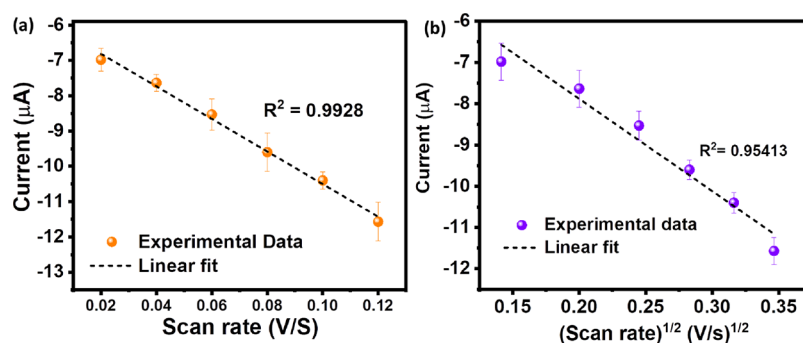
Figure 5. Liner regression fitting for the anodic peak current against scan rate (a) adsorption and (b) diffusion-controlled electrochemical reduction of 4-NP by *MXene*.

that exfoliated *MXene* contains surface-active functional groups and adsorption of moieties along with the presence of minute reaction byproducts.[43] Finally, the deconvoluted F 1s spectrum assigned at 684.87, 685.73, 686.39, and 687.99 eV (Figure 3e) corresponding to C-Ti-F$_x$, TiO$_{2-x}$F$_x$, AlFx, and Al(*OF*)x, respectively, indicates the attachment of the −F functional element during the exfoliation and formation of reaction byproducts.[44−46] Thus, the results of the XPS analysis confirm the evolution of the exfoliation of the Ti$_3$C$_2$T$_x$-*MXene* layered structure along with surface-active groups and edges from the ceramic MAX phase on chemical etching. Further, the measured specific surface area (see Figure S4) and the average pore size of the exfoliated *MXene* are 7.8 m^2/g and 19.5 nm, respectively, which are similar to the previously reported values.[47] As we will see below, the effectively exfoliated *MXene* possesses high sensitivity and a low detection limit of 4-NP in the electrochemical detection.

2.2. Electrochemical Behavior of *MXene*. The electrochemical tests of the bare GCE and *MXene*-coated GCE (*MXene*/GCE) were performed in a standard electrochemical cell system with 0.1 M PBS used as the electrolyte solution. Figure 4a presents the cyclic voltammetry (CV) of tested electrodes with a scan rate of 100 mV/s in similar testing conditions. As seen in the figure, the peak current intensity of *MXene*/GCE electrodes was significantly larger compared with that of the bare GCE, indicating an accelerated rate of electron transfer due the superior electrical conductivity along with a notable surface area of *MXene*.[28,45] In addition to that, the CV test was conducted to analyze the electrochemical activity of *MXene*-modified GCE electrodes toward 4-NP (total concentration ≈ 100 μM/L) in PBS (0.1 M) electrolyte at pH 3. Before addition of 4-NP into the electrolyte solution, no considerable changes in the oxidation and reduction peak were observed for both tested electrodes. After the addition of 4-NP, the *MXene*-modified electrode displays an anodic peak in the potential range from −0.85 to −0.90 V/s as shown in Figure 4a. The observed irreversible anodic peak current for *MXene*/GCE electrodes strongly explains the conversion of 4-NP to 4-hydroxyaminophenol (4-HAP) by a direct reduction process of four electrons and a four proton transfer process (Figure 4b).[6,48,49] The possible catalytic electrochemical reaction and sensing mechanism of the prepared *MXene*-modified electrodes and subsequent reduction process of 4-NP are given by eqs 1 and 2.

$$\text{Ti}_3\text{C}_2\text{T}_x + 4e^- \rightarrow (\text{Ti}_3\text{C}_2\text{T}_x)^{4-} \tag{1}$$

$$(\text{Ti}_3\text{C}_2\text{T}_x)^{4-} + 4 - \text{NP} + 4\text{H}^+$$
$$\rightarrow \text{Ti}_3\text{C}_2\text{T}_x + 4 - \text{HAP} + \text{H}_2\text{O} \tag{2}$$
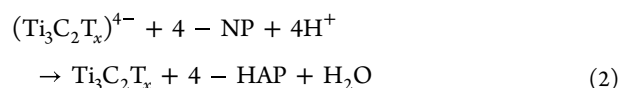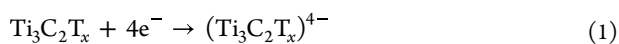
In the above catalytic reaction, first, *MXene* (Ti$_3$C$_2$T$_x$) was electrochemically reduced into (Ti$_3$C$_2$T$_x$)$^{4-}$. Subsequently, 4-NP was chemically reduced to 4-hydroxylaminophenol (4-HAP). Note that we did not observe any cathodic peaks for the reversible reaction leading to the transformation of 4-HAP to 4-NP. The interesting aspects of electrochemical conversion of 4-NP to 4-HAP using exemplary *MXene* layer materials can be explained as follows: The surface-exposed titanium atoms combined with a robust carbon elemental composition of Ti$_3$C$_2$T$_x$ create more conducting channels for electron transport.[49,50] The stacked layers of bulk *MXene* exfoliated from MAX form accordion-like structures, preferably having more surface reactive sites, which facilitate both electrolyte and electron transfer without any barrier during the electrochemical reaction process.[10] Inherently, the abundance of active functional groups such as −OH, −F, and ═O leading to the negative surface charges of *MXene* benefits the sensing of positively charged analytes.[11,50,51] Therefore, the synthesized *MXene* layered structure displayed an enhanced electrochemical performance and catalytic reduction and was a more affordable candidate for electrochemical detection of 4-NP. We emphasize here that the above observed four-electron catalytic reduction process of our *MXene* is a result of quality *MXene* layer synthesis following our synthesis protocols.

To explore the optimum pH condition to evaluate the electrochemical reaction of *MXene*-modified electrodes for reduction of 4-NP, electrochemical CV measurements of *MXene*/GCE electrodes were further performed under different pH conditions in the presence of 4-NP (100 μM) at pH 3, 5, and 7, as shown in Figure 4b. The recorded CV curve at pH 3 showed a distinct anodic peak current value in the potential range from −0.85 to −0.90 V compared with other (5 and 7) pH conditions. As plotted in Figure S5, the linear relationships between the pH and oxidation peak potential (E_p), with a slope value of 49 mV, demonstrate an ideal theoretical value (59 mV), revealing an equal number of electrons and protons involved in the catalytic oxidation process. From Figure S5, it can be observed that the very distinct oxidation peak current of 4-NP at pH 3 (this optimum pH condition for the electrochemical reactions of *MXene* with 4-NP was thus chosen for sensing experiments in our work). Based on this near ideal catalytic reduction process, the pH 3 value at the *MXene* surface facilitates an equal number of 4-NP molecular conversion as the latter one finally converts to the same
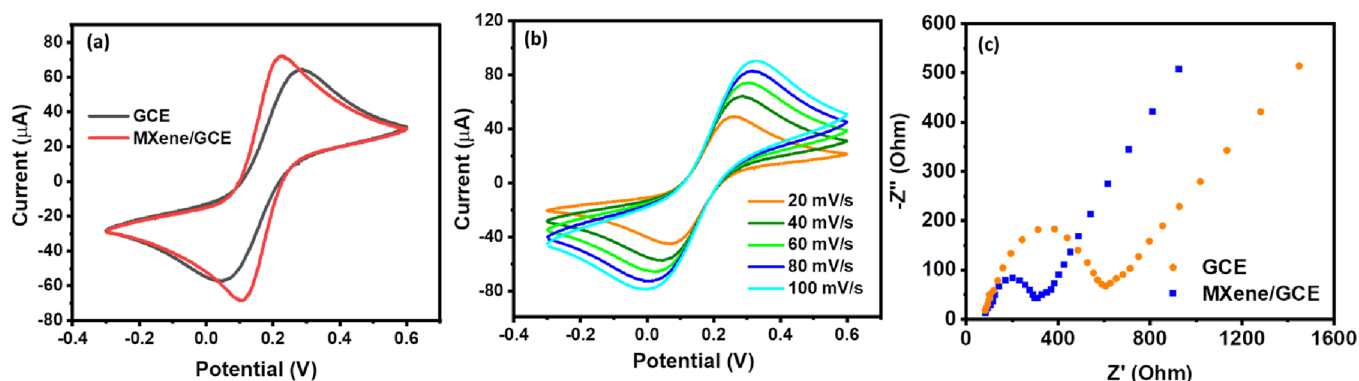
Figure 6. (a, b) CV of GCE and *MXene*/GCE electrodes at different scan rates in 5 mM $[\mathrm{Fe(CN)_6}]^{3-/4-}$ containing 0.1 M KCl and (c) Nyquist plot of electrochemical impedance of bare GCE and *MXene*-modified GCE measured in the frequency range between 0.01 and 100 kHz rates in 5 mM $[\mathrm{Fe(CN)_6}]^{3-/4-}$ containing 0.1 M KCl.
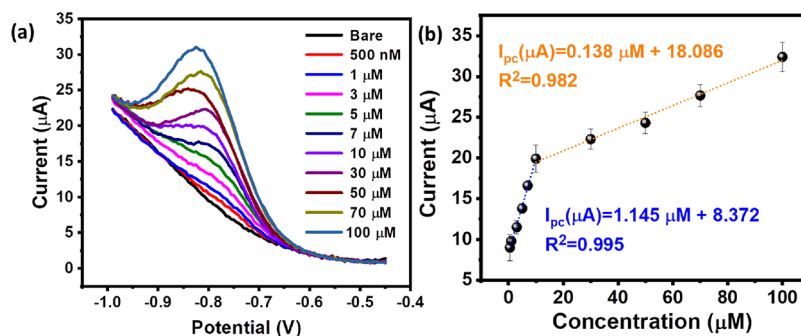
Figure 7. (a) DPV curves of the prepared *MXene* sensor electrodes for different concentrations of 4-NP from 500 nM to 100 μM measured at 25 mV/s and (b) consequent calibration plot between reduction DPV peak current readings and known concentrations of 4-NP with a linear regression analysis fit.

number of 4-hydroxy aminophenol; please see Figure 4b for the schematic representation of the catalytic process. The effect of scan rate (20 to 120 mV/s) on the anodic peak current of fabricated *MXene*/GCE electrodes was measured using CV to explore the reaction kinetics in the presence of 100 μM 4-NP concentration. As shown in Figure 4c, the peak reduction current gradually increased upon increasing the scan rate from 20 to 120 mV/s along with slight shifting of the irreversible reduction peak potential toward negative values, indicating irreversibility in electrochemical reduction of 4-NP occurring at the *MXene*/GCE electrode surface. In order to understand the mechanism and kinetics of charge transfer between 4-NP molecules and *MXene* sensor during the above irreversible reduction processes, the cathodic current was further analyzed by plotting the peak current vs scan rates and peak current vs square root of the scan rates, respectively. Figure 5 shows the comparison of peak current fitting with scan rate as well as the square root of the scan rate of voltametric cycling operation. Results indicate that the cathodic current sensed by *MXene* electrodes is an adsorption-controlled process ($R^2 = 0.9928$) in contrast to a diffusion controlled one ($R^2 = 0.9541$). This explains that much of the molecule transport occurs from the aqueous bulk to the interface.[52] The electrochemical behavior of GCE and *MXene*/GCE electrodes was investigated via CV in a standard redox probe of 5 mM $[\mathrm{Fe(CN)6}]^{3-/4-}$ aqueous solution containing 0.1 M KCl. As supported by Figure 6a,b, modification of *MXene* increased the peak current of the GCE. In addition, an increasing peak current for higher scan rates was observed for *MXene*/GCE electrodes. In addition to

that, electrochemical impedance spectroscopy (EIS) of the bare GCE and *MXene*-modified GCE was performed in a standard redox probe of 5 mM $[\mathrm{Fe(CN)6}]^{3-/4-}$ aqueous solution containing 0.1 M KCl. From EIS measurements, the charge transfer resistance (R_{ct}) between the electrode surface and the solution was extracted from the size of the semicircle in the Nyquist impedance plot based on Randles' equivalent circuit model. As shown in Figure 6c, the *MXene*/GCE electrodes show a smaller semicircle with a low charge transfer resistance ($R_{ct} \sim 249.34$ Ω), much lower compared with those from the bare GCE ($R_{ct} \approx 527.01$ Ω).[53] This is attributed to an accelerated electron transfer between the electrode surface and solution by *MXene* materials. With the low resistivity feature of $\mathrm{Ti_3C_2T_x}$ compared to the GCE, the overall conductivity of the modified working electrode (*MXene*/GCE) drastically increases, leading to a high electron transfer. This also demonstrates the role of *MXene* as a conducting platform for charge transport in addition to serving as an active material for electrochemical reduction of 4-NP.[54−58] Electrochemical analysis explicitly gives evidence that the chemically exfoliated $\mathrm{Ti_3C_2T_x}$*MXene* material is a highly desirable material for electrochemical reduction of 4-NP in the environment.

2.3. Sensitivity and Limit of Detection. The quantitative analysis of different 4-NP concentrations, including the detection limit, using *MXene*/GCE electrodes was studied by differential pulse voltammetry (DPV) technique. Figure 7a,b shows the DPV response of the electrochemical reduction of 4-NP using *MXene*/GCE electrodes at 0.1 M PBS (pH 3). As expected, the DPV peak current increased gradually upon continuous addition of 4-NP, which indicates the rapid

Table 1. Comparison Analysis of Recently Reported NP Sensing by Novel Materials

electrode materials	linear range (μM/L)	sensitivity (μA μM^{-1} cm^{-2})	LOD (μM/L)	method	repeatability (RSD%)	recoveries in real samples (%)	ref
graphene/acetylene black/CPE	0.02−8	2.717	0.08	DPV	2.75	97.4−103.5	6
graphene-chit/acetylene black/CPE	0.4−80	1.480	0.08	LSV	5.04	96.0−103.5	23
graphene-AuNP/GCE	0.036−90	0.1134	0.01	LSV	3.9	97.8−103.9	66
hydroxyapatite/GCE	1−300	0.0295	0.6	DPV		95.9−104.4	67
AgNWs with PANI/GCE	0.6−32	14.6	0.025	DPV		97.0−101.5	68
carbon black/β-CD/GCE	0.125−225	9.2	0.040	DPV		96.2−98.6	69
tyrosinase/*MXene*/GCE	0.05−15.5	0.414	0.012	Amperometry	1.3	86.8−106	28
Nb$_2$CTX/ Zn-Co-N/GCE	1−500	4.65	0.070	DPV	0.97		29
Pt@Ti$_3$C$_2$T$_x$	0.5−5		0.032	DPV	2.1	92.1−94.5	31
multilayer Ti$_3$C$_2$T$_x$	0.5−25	1.22	0.11	DPV			32
Ti$_3$C$_2$T$_x$	0.5−100	16.35	0.042	DPV	1.44	95.09−99.15	this work
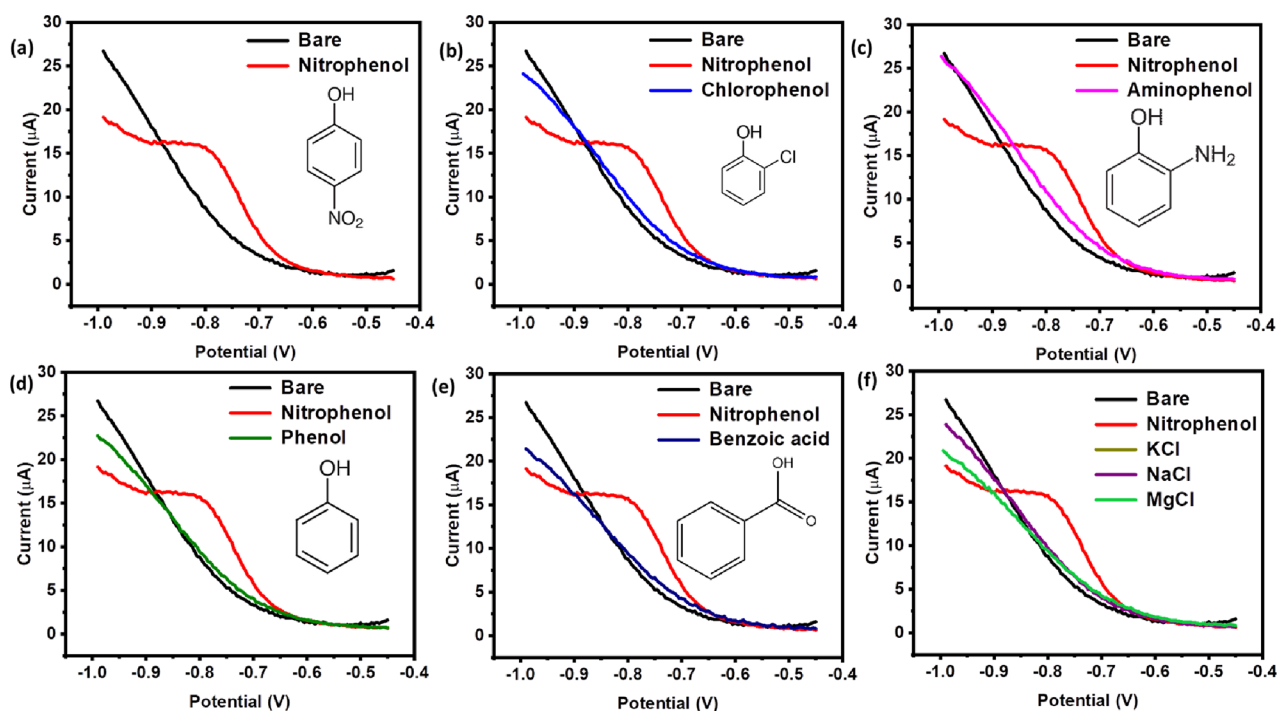
Figure 8. DPV curves of 5 μM 4-NP measured at 25 mV/s in 0.1 M PBS (pH 3) of the prepared *MXene*/GCE electrodes in comparison with presence of (b) 50 μM chlorophenol, (c) 50 μM aminophenol, (d) 50 μM phenol, (e) 50 μM benzoic acid, and (f) ionic interference (each 50 μM of KCl, NaCl, and MgCl).

electrochemical reduction of 4-NP by *MXene* electrodes (Figure 7a). In addition, the linear regression analysis of subjected 4-NP concentrations was fitted with respective peak current values as given in Figure 7b. The resulting correlation shows two linear sensing regimes (corresponding to a linear relationship between the DPV peak current change vs 4-NP concentration) for 4-NP with correlation coefficients of 0.995 and 0.985. The first regime corresponds to a concentration window of 0 to 10 μM and the second one corresponds to a concentration window of 10 to 100 μM 4-NP. Furthermore, comparing the slopes of two sensing regimes, the fabricated *MXene*/GCE electrodes show more sensitivity at the lower concentration window compared to the higher concentration window.[31,59] The electrochemical chemical reduction of 4-NP on the surface of exfoliated stacked *MXene* was hindered at higher concentrations due to the decreased active sites by the irreversible adsorption controlled process. The calculated

sensitivity, limit of quantification (LOQ), and limit of detection (LOD) are about 16.357 μA μM^{-1} cm^{-2}, 0.1517 μM/L, and 45.34 $\pm$ 1.96 nM/L, respectively, from the standard formula.[60] Table 1 provides a comprehensive summary of nitrophenol detection using different electrochemical sensors with *MXene* and other 2D materials. Our experimental result demonstrates it to be one of the best 4-NP sensors in terms of performance that is substantially lower than the permitted limits of 4-NP in drinking water. Therefore, chemically exfoliated stacked Ti$_3$C$_2$T$_x$*MXene* layers show excellent electrochemical and catalytic activity with a great linear response and lower LOD toward detection of 4-NP.

2.4. Selectivity, Interference, Reproducibility, and Real-Time Analysis of the *MXene* 4-NP Sensor. Reliability, reproducibility, interference with other environmental analytes, and real-time detection methodology development are key components of sensor technologies that prompted us to further
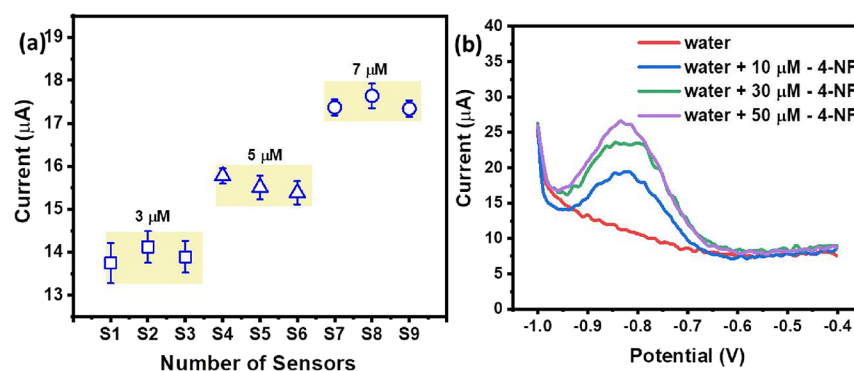
Figure 9. (a) Stability analysis of *MXene*/GCE toward 4-NP detection and (b) real-time 4-NP detection in water samples by DPV techniques measured at 0.1 M PBS (pH 3).

extend the present study to identifying the potential of the *MXene* 4-NP sensor. Experiments were performed to study the selectivity of the *MXene* sensor using DPV technique with the introduction of similar derivatives to 4-NP such as chlorophenol, aminophenol, phenol, benzoic acid, and cations such as K^+, Na^+, and Mg^+. As given in Figure 8a–f, negligible changes in the reduction peak current were observed in the presence of homologues of 4-NP, even at higher concentrations. This is attributed to the fact that our *MXene* sensor is indeed more selective to 4-NP. The interference study was also conducted by comparing DVP current signals with and without addition of some common interfering inorganic ions, and their corresponding DPV curves are presented in Figure 8f. It can be observed that the discriminating ability *MXene* toward 4-NP was not influenced in the existence of Na^+, K^+, and Mg^{2+} tested under 50 μM/L dosage. As summarized in Table S1, the interfering phenolic derivatives and common metal ions have a smaller effect (<6%) on the detection of 4-NP. These results clearly indicate that the fabricated *MXene* electrochemical sensor possesses excellent selectivity and higher sensitivity along with inertness toward common interfering agents in water.[61–63] The selectivity toward 4-NP over other phenolic interference derivatives can be explained as follows: During the chemical exfoliation process, a number of surface-active functional groups such as −OH and −F get anchored on the *MXene* surface and these active groups are more favorable for specific reactions with 4-NP in a mixed environment during the reduction process. During the electrochemical reaction, the nitro group in 4-NP (in the *para* position with respect to the hydroxyl group) readily underwent an electrophilic substitution by the −OH group, leading to the conversion of 4-NP to 4-hydroxyaminophenol (see Figure 4b) without intermediate formation.[64] This electrophilic substitution reaction only occurred in 4-NP and not with other similar phenolic derivatives, explaining the selectivity of 4-NP to others in Figure 8. The operational repeatability of the electrochemical sensor was evaluated by using DPV techniques for the three similarly prepared *MXene*/GCE electrodes tested for 3 μM/L, 5 μM/L, and 7 μM/L 4-NP detection. The results indicate no considerable variation in the oxidation peak−current response as shown in Figure 9a and Figure S6. Moreover, the fabricated electrodes show a relative standard deviation (RSD) of ~1.44% for three independent successive measurements, thereby suggesting a good reproducibility of the *MXene* environmental electrochemical sensor for 4-NP detection. The stability of the *MXene* was tested by doing electrochemical cycling at three different concentrations with three times

recycling at each concentration and then characterizing the *MXene* material by SEM (the material was gently scratched from the electrode surface, and its SEM was performed). As supported by the SEM image (Figure S6), the stacked *MXene* structure remains intact after multiple sensing experiments. Additionally, minimal changes in the chemical stoichiometry after sensing experiments, as probed by TEM and EDS measurement (Figure S6), further strengthen *MXene*'s sensing application. Further detailed experimental studies are required to fully understand the structure−property relations of *MXene* electrodes during catalytic reduction of 4-NP.[65] Finally, the fabricated *MXene*/GCE sensors were tested in natural water such as tap water modified at pH 3 (in accordance with the maximum signal shown in Figure 4a,c) to establish their selectivity within real environmental matrices. While we intend to further explore developing water-based nitrophenol sensors at other pH values, the reported result in this work is particularly important to test the water samples in a low pH soil−water system, causing consumption of certain water-borne metals in plant intakes. This vital global environmental issue is of concern. Different amounts of 4-NP were spiked into the tap water samples containing various known concentrations. The DPV technique was applied to detect the reduction peak current of the tap water samples with different 4-NP contents. As supported by Figure 9b, the fabricated *MXene*/GCE electrode has discrete anodic peak currents with respect to the concentration. Moreover, as shown in Table 2,

Table 2. Determination of the 4-NP in Real Tap Water Samples

real sample	NP added (μM)	NP detected (μM)	recovery (%)	RSD[a] (%)
tap water	10	9.500	95.09	2.73
	30	29.21	97.39	3.33
	50	49.573	99.15	1.64

[a]Relative standard deviation (n = 3).

the protocol for recovery analysis was applied to further strengthen the applicability of the fabricated 4-NP electrochemical *MXene* sensor in aqueous media. The *MXene* sensors demonstrated a recovery percentage between 95 and 99 with a relative standard deviation of 1.6 to 3.3%.

3. CONCLUSIONS

In conclusion, a novel and reliable $Ti_3C_2T_x$-based *MXene* electrochemical sensor was successfully developed for selective

identification of 4-NP in water via catalytic reduction pathways. Although acid-based etching of metal atoms and exfoliation of the MAX phase material is widely employed for 2D *MXene* synthesis, we emphasize a selective chemical etching and exfoliation producing quality *MXene* layers as a key to achieving high-quality 4-NP sensors. These sensors follow an underlying adsorption mechanism of the charge transfer process. The fabricated *MXene*/GCE sensors exhibited an excellent electrochemical performance to detect 4-NP with a superior sensitivity of 16.370 $\mu A\ \mu M^{-1}\ cm^{-2}$ and low detection limit as low as 0.04 μM. The chemically exfoliated stacked *MXene* structure promoted the formation of efficient charge-transport layer due to its excellent electrical conductivity and also exhibited an active role in the catalytic reaction during reduction of 4-NP. Furthermore, the sensors have successfully demonstrated reliability, reproducibility, and the continuous monitoring of 4-NP in tap water samples with negligible interference from frequent interfering species. Overall, $Ti_3C_2T_x$-based pure *MXene* promises a reliable noninvasive advanced nanomaterial for 4-NP environmental pollutants in soils and the water network.

4. EXPERIMENTAL SECTION

4.1. Synthesis of 2D *MXene*. Layered stacked *MXene* ($Ti_3C_2T_x$) was synthesized from 3D ceramic MAX (Ti_3AlC_2) phase materials using selective removal of the Al layer in the presence of strong etchant hydrofluoric acid solution (HF, >49%).[37,46] Initially, 5 wt % MAX phase powders were gently mixed with the desired amount of etchant solution. The careful step-by-step addition of MAX powder into the HF solution is mandatory in order to avoid a violent exothermic reaction. The etching reaction was performed at 50 °C for about 36 h under continuous stirring conditions. After completion of the etching experiment, the exfoliated *MXene* was extracted by continuous washing with water via centrifugation at 3500 rpm for 10 min. The washing cycles were repeated with a copious amount of water until the pH of the supernatant reached between 5 and 6. The obtained *MXene* slurry was again washed with water and ethanol during vacuum filtration (0.22 μm pore size PTFE membrane). The final cake-like wet *MXene* was vacuum-dried at 27 °C for 48 h to get final dried *MXene* powders that were stored in a vacuum desiccator to avoid oxidation. The resulting *MXene* powders were used for electrochemical experiments without further modification or processing.

4.2. Characterization. The morphological feature of exfoliated *MXene* was observed from a scanning electron microscope (FESEM, SU8010, Hitachi) inbuilt with an energy-dispersive spectroscope (EDS). Assembly of the different stacked layer structures of *MXene* was further characterized using transmission electron microscopy (TEM) using an FEI Tecnai G230. The crystalline structural features of *MXene* after chemical exfoliation were examined using an X-ray diffractometer (XRD, PANalytical, X'Pert PRO, Netherlands) with Cu Kα radiation (λ = 1.54 Å) operated at 30 kV at a measured step size of 0.05°. The elemental distribution of exfoliated *MXene* was characterized using X-ray photoelectron spectroscopy (XPS, Thermo Scientific ESCALAB 250Xi, UK).

4.3. Electrochemical Measurements. In this work, all electrochemical studies on *MXene* were performed using the three electrode systems with a controlled electrochemical analyzer (Biologics SP-150). The *MXene*-coated glassy carbon electrode hereafter referred to as *MXene*/GCE was used as the working electrode. A platinum wire (Pt) and 3 M KCl statured

Ag/AgCl electrodes served as the counter and reference electrodes, respectively, throughout the experiments. *MXene*-coated GCE electrodes were prepared as follows: the desired amount of slurry *MXene* was prepared by dispersing *MXene* powder (5 mg) into ethanol (2 mL) and then subjecting to a 30 min bath sonication. Subsequently, 5 μL of aliquot was dropped onto to the pre-cleaned GCE, then allowed to air dry for about 30 min, and then washed with 0.1 M phosphate buffer solution (PBS). The electrochemical analysis was conducted in 0.1 M PBS solution at 25 ± 2 °C. Cyclic voltammetry (CV) and electrochemical impedance spectroscopy (EIS) were used to study the electrochemical performance of pure and *MXene*-modified GCE electrodes in the electrolyte containing 5 mM $[Fe(CN)_6]^{3-/4-}$ in 0.1 M KCl. The frequency range is between 0.01 and 100 kHz, and the amplitude is 5 mV. All electrochemical analyses were performed more than three times, and the results are presented in standard error.

■ ASSOCIATED CONTENT

ⓢ Supporting Information

The Supporting Information is available free of charge at https://pubs.acs.org/doi/10.1021/acsomega.2c06505.

> Additional figures (SEM and HR-TEM characterization of the MAX materials, XPS full survey spectrum, and BET analysis), selectivity, interference study, and reproducibility test of the *MXene*/GCE sensor (PDF)

■ AUTHOR INFORMATION

Corresponding Author

Suprem R Das − *Department of Industrial and Manufacturing Systems Engineering and Department of Electrical and Computer Engineering, Kansas State University, Manhattan, Kansas 66506, United States;* ⓘ orcid.org/0000-0003-0334-7600; Phone: (785) 532-5606; Email: srdas@ksu.edu

Authors

Rajavel Krishnamoorthy − *Department of Industrial and Manufacturing Systems Engineering, Kansas State University, Manhattan, Kansas 66506, United States*

Karuppasamy Muthumalai − *Advanced Materials and Devices Laboratory (AMDL), Department of Nanoscience and technology, Bharathiar University, Coimbatore 641 046 Tamil Nadu, India*

Thiba Nagaraja − *Department of Industrial and Manufacturing Systems Engineering, Kansas State University, Manhattan, Kansas 66506, United States*

Ramasamy Thangavelu Rajendrakumar − *Advanced Materials and Devices Laboratory (AMDL), Department of Nanoscience and technology, Bharathiar University, Coimbatore 641 046 Tamil Nadu, India;* ⓘ orcid.org/0000-0002-4188-5859

Complete contact information is available at:
https://pubs.acs.org/10.1021/acsomega.2c06505

Notes

The authors declare no competing financial interest.

■ REFERENCES

(1) Xiong, Z.; Zhang, H.; Zhang, W.; Lai, B.; Yao, G. Removal of nitrophenols and their derivatives by chemical redox: A review. *Chem. Eng. J.* **2019**, *359*, 13−31.

(2) Tchieno, F. M. M.; Tonle, I. K.p-Nitrophenol determination and remediation: an overview. *Rev. Anal. Chem.* **2018**, *37* (), 10.1515/revac-2017-0019.

(3) Musilová, J.; Barek, J.; Pecková, K. Determination of Nitrophenols in Drinking and River Water by Differential Pulse Voltammetry at Boron-Doped Diamond Film Electrode. *Electroanalysis* **2011**, *23*, 1236−1244.

(4) Nthunya, L. N.; Masheane, M. L.; Malinga, S. P.; Nxumalo, E. N.; Mhlanga, S. D. Electrospun chitosan-based nanobres for removal of phenols from drinking water. *Water Sa* **2018**, *44*, 377−386.

(5) Prabakaran, E.; Pillay, K. Electrochemical Detection of 4-Nitrophenol by Using Graphene Based Nanocomposite Modified Glassy Carbon Electrodes: A Mini Review. *NANO* **2021**, 61−87.

(6) He, Q.; Tian, Y.; Wu, Y.; Liu, J.; Li, G.; Deng, P.; Chen, D. Facile and ultrasensitive determination of 4-nitrophenol based on acetylene black paste and graphene hybrid electrode. *Nanomaterials* **2019**, *9*, 429.

(7) Rajkumar, C.; Veerakumar, P.; Chen, S.-M.; Thirumalraj, B.; Lin, K.-C. Ultrathin sulfur-doped graphitic carbon nitride nanosheets as metal-free catalyst for electrochemical sensing and catalytic removal of 4-nitrophenol. *ACS Sustainable Chem. Eng.* **2018**, *6*, 16021−16031.

(8) Tecuapa-Flores, E. D.; Hernández, J. G.; Roquero-Tejeda, P.; Arenas-Alatorre, J. A.; Thangarasu, P. Rapid electrochemical recognition of trimethoprim in human urine samples using new modified electrodes (CPE/Ag/Au NPs) analysing tunable electrode properties: experimental and theoretical studies. *Analyst* **2021**, *146*, 7653−7669.

(9) Schaider, L. A.; Rudel, R. A.; Ackerman, J. M.; Dunagan, S. C.; Brody, J. G. Pharmaceuticals, perfluorosurfactants, and other organic wastewater compounds in public drinking water wells in a shallow sand and gravel aquifer. *Sci. Total Environ.* **2014**, *468*, 384−393.

(10) Kalambate, P. K.; Gadhari, N. S.; Li, X.; Rao, Z.; Navale, S. T.; Shen, Y.; Patil, V. R.; Huang, Y. Recent advances in MXene−based electrochemical sensors and biosensors. *TrAC, Trends Anal. Chem.* **2019**, *120*, 115643.

(11) Sajid, M. MXenes: are they emerging materials for analytical chemistry applications?−A review. *Anal. Chim. Acta* **2021**, *1143*, 267−280.

(12) Huang, H.; Jiang, R.; Feng, Y.; Ouyang, H.; Zhou, N.; Zhang, X.; Wei, Y. Recent development and prospects of surface modification and biomedical applications of MXenes. *Nanoscale* **2020**, *12*, 1325−1338.

(13) Rajavel, K.; Shen, S.; Ke, T.; Lin, D. Achieving high bactericidal and antibiofouling activities of 2D titanium carbide (Ti3C2Tx) by delamination and intercalation. *2D Materials* **2019**, *6*, No. 035040.

(14) Ronchi, R. M.; Arantes, J. T.; Santos, S. F. Synthesis, structure, properties and applications of MXenes: current status and perspectives. *Ceram. Int.* **2019**, *45*, 18167−18188.

(15) Bu, F.; Zagho, M. M.; Ibrahim, Y.; Ma, B.; Elzatahry, A.; Zhao, D. Porous MXenes: Synthesis, structures, and applications. *Nano Today* **2020**, *30*, 100803.

(16) Xia, Z.; Huang, Q.; Guo, S. Recent progress on synthesis, structure and electrocatalytic applications of MXenes. *FlatChem* **2019**, *17*, 100129.

(17) Kumar, J. A.; Prakash, P.; Krithiga, T.; Amarnath, D. J.; Premkumar, J.; Rajamohan, N.; Vasseghian, Y.; Saravanan, P.; Rajasimman, M. Methods of synthesis, characteristics, and environmental applications of Mxene: A comprehensive review. *Chemosphere* **2022**, *286*, 131607.

(18) Fan, Y.; Li, L.; Zhang, Y.; Zhang, X.; Geng, D.; Hu, W. Recent advances in growth of transition metal carbides and nitrides (MXenes) crystals. *Adv. Funct. Mater.* **2022**, *32*, 2111357.

(19) Ramanavicius, S.; Ramanavicius, A. Progress and insights in the application of MXenes as new 2D nano-materials suitable for biosensors and biofuel cell design. *Int. J. Mol. Sci.* **2020**, *21*, 9224.

(20) Naguib, M.; Mashtalir, O.; Carle, J.; Presser, V.; Lu, J.; Hultman, L.; Gogotsi, Y.; Barsoum, M. W. Two-dimensional transition metal carbides. *ACS Nano* **2012**, *6*, 1322−1331.

(21) Hu, T.; Yang, J.; Wang, X. Carbon vacancies in Ti2CT2 MXenes: defects or a new opportunity? *Phys. Chem. Chem. Phys.* **2017**, *19*, 31773−31780.

(22) Hart, J. L.; Hantanasirisakul, K.; Lang, A. C.; Anasori, B.; Pinto, D.; Pivak, Y.; van Omme, J. T.; May, S. J.; Gogotsi, Y.; Taheri, M. L. Control of MXenes' electronic properties through termination and intercalation. *Nat. Commun.* **2019**, *10*, 1−10.

(23) Deng, P.; Xu, Z.; Li, J. Simultaneous voltammetric determination of 2-nitrophenol and 4-nitrophenol based on an acetylene black paste electrode modified with a graphene-chitosan composite. *Microchim. Acta* **2014**, *181*, 1077−1084.

(24) Wu, X.; Ma, P.; Sun, Y.; Du, F.; Song, D.; Xu, G. Application of MXene in electrochemical sensors: a review. *Electroanalysis* **2021**, *33*, 1827−1851.

(25) Alhabeb, M.; Maleski, K.; Anasori, B.; Lelyukh, P.; Clark, L.; Sin, S.; Gogotsi, Y. Guidelines for Synthesis and Processing of Two-Dimensional Titanium Carbide (Ti3C2Tx MXene). *Chem. Mater.* **2017**, *29*, 7633−7644.

(26) Eom, W.; Shin, H.; Ambade, R. B.; Lee, S. H.; Lee, K. H.; Kang, D. J.; Han, T. H. Large-scale wet-spinning of highly electroconductive MXene fibers. *Nat. Commun.* **2020**, *11*, 1−7.

(27) Rhouati, A.; Berkani, M.; Vasseghian, Y.; Golzadeh, N. MXene-based electrochemical sensors for detection of environmental pollutants: A comprehensive review. *Chemosphere* **2022**, 132921.

(28) Wu, L.; Lu, X.; Wu, Z. S.; Dong, Y.; Wang, X.; Zheng, S.; Chen, J. 2D transition metal carbide MXene as a robust biosensing platform for enzyme immobilization and ultrasensitive detection of phenol. *Biosens. Bioelectron.* **2018**, *107*, 69−75.

(29) Huang, R.; Liao, D.; Liu, Z.; Yu, J.; Jiang, X. Electrostatically assembling 2D hierarchical Nb2CTx and zifs-derivatives into Zn-Co-NC nanocage for the electrochemical detection of 4-nitrophenol. *Sens. Actuators, B* **2021**, *338*, 129828.

(30) Yun, T.; Kim, H.; Iqbal, A.; Cho, Y. S.; Lee, G. S.; Kim, M.-K.; Kim, S. J.; Kim, D.; Gogotsi, Y.; Kim, S. O.; Koo, C. M. Electromagnetic Shielding of Monolayer MXene Assemblies. *Adv. Mater.* **2020**, *32*, 1906769.

(31) Rasheed, P. A.; Pandey, R. P.; Jabbar, K. A.; Mahmoud, K. A. Platinum nanoparticles/Ti3C2Tx (MXene) composite for the effectual electrochemical sensing of Bisphenol A in aqueous media. *J. Electroanal. Chem.* **2021**, *880*, 114934.

(32) Lei, L.; Li, C.; Huang, W.; Wu, K. Simultaneous detection of 4-chlorophenol and 4-nitrophenol using a Ti 3 C 2 T x MXene based electrochemical sensor. *Analyst* **2021**, *146*, 7593−7600.

(33) Rajavel, K.; Ke, T.; Yang, K.; Lin, D. Condition optimization for exfoliation of two dimensional titanium carbide (Ti3C2Tx). *Nanotechnology* **2018**, *29*, No. 095605.

(34) Rajavel, K.; Luo, S.; Wan, Y.; Yu, X.; Hu, Y.; Zhu, P.; Sun, R.; Wong, C. 2D Ti3C2Tx MXene/polyvinylidene fluoride (PVDF) nanocomposites for attenuation of electromagnetic radiation with excellent heat dissipation. *Composites Part A: Applied Science and Manufacturing* **2020**, *129*, 105693.

(35) Dong, Y.; Wu, Z.-S.; Zheng, S.; Wang, X.; Qin, J.; Wang, S.; Shi, X.; Bao, X. Ti3C2 MXene-derived sodium/potassium titanate nanoribbons for high-performance sodium/potassium ion batteries with enhanced capacities. *ACS Nano* **2017**, *11*, 4792−4800.

(36) Khan, A. R.; Husnain, S. M.; Shahzad, F.; Mujtaba-ul-Hassan, S.; Mehmood, M.; Ahmad, J.; Mehran, M. T.; Rahman, S. Two-dimensional transition metal carbide (Ti3C2Tx) as an efficient adsorbent to remove cesium (Cs+). *Dalton Trans.* **2019**, *48*, 11803−11812.

(37) Mahmood, M.; Rasheed, A.; Ayman, I.; Rasheed, T.; Munir, S.; Ajmal, S.; Agboola, P. O.; Warsi, M. F.; Shahid, M. Synthesis of

ultrathin MnO2 nanowire-intercalated 2D-MXenes for high-performance hybrid supercapacitors. *Energy Fuels* **2021**, *35*, 3469−3478.

(38) Chen, J.; Yuan, X.; Lyu, F.; Zhong, Q.; Hu, H.; Pan, Q.; Zhang, Q. Integrating MXene nanosheets with cobalt-tipped carbon nanotubes for an efficient oxygen reduction reaction. *J. Mater. Chem. A* **2019**, *7*, 1281−1286.

(39) Feng, A.; Yu, Y.; Wang, Y.; Jiang, F.; Yu, Y.; Mi, L.; Song, L. Two-dimensional MXene Ti3C2 produced by exfoliation of Ti3AlC2. *Mater. Des.* **2017**, *114*, 161−166.

(40) Li, Z.; Wang, L.; Sun, D.; Zhang, Y.; Liu, B.; Hu, Q.; Zhou, A. Synthesis and thermal stability of two-dimensional carbide MXene Ti3C2. *Mater. Sci. Eng., B* **2015**, *191*, 33−40.

(41) Liu, Y.; Zhang, X.; Dong, S.; Ye, Z.; Wei, Y. Synthesis and tribological property of Ti3C2TX nanosheets. *J. Mater. Sci.* **2017**, *52*, 2200−2209.

(42) Halim, J.; Cook, K. M.; Naguib, M.; Eklund, P.; Gogotsi, Y.; Rosen, J.; Barsoum, M. W. X-ray photoelectron spectroscopy of select multi-layered transition metal carbides (MXenes). *Appl. Surf. Sci.* **2016**, *362*, 406−417.

(43) Tanuma, T.; Okamoto, H.; Ohnishi, K.; Morikawa, S.; Suzuki, T. Partially fluorinated metal oxide catalysts for a Friedel−Crafts-type reaction of dichlorofluoromethane with tetrafluoroethylene. *Catal. Lett.* **2010**, *136*, 77−82.

(44) Mashtalir, O.; Naguib, M.; Dyatkin, B.; Gogotsi, Y.; Barsoum, M. W. Kinetics of aluminum extraction from Ti3AlC2 in hydrofluoric acid. *Mater. Chem. Phys.* **2013**, *139*, 147−152.

(45) Sultana, T.; Georgiev, G. L.; Auner, G.; Newaz, G.; Herfurth, H. J.; Patwa, R. XPS analysis of laser transmission micro-joint between poly (vinylidene fluoride) and titanium. *Appl. Surf. Sci.* **2008**, *255*, 2569−2573.

(46) Zhao, D.; Chen, Z.; Yang, W.; Liu, S.; Zhang, X.; Yu, Y.; Cheong, W.-C.; Zheng, L.; Ren, F.; Ying, G.; Cao, X.; Wang, D.; Peng, Q.; Wang, G.; Chen, C. MXene (Ti3C2) vacancy-confined single-atom catalyst for efficient functionalization of CO2. *J. Am. Chem. Soc.* **2019**, *141*, 4086−4093.

(47) Xia, Q. X.; Fu, J.; Yun, J. M.; Mane, R. S.; Kim, K. H. High volumetric energy density annealed-MXene-nickel oxide/MXene asymmetric supercapacitor. *RSC Adv.* **2017**, *7*, 11000−11011.

(48) Mathew, M.; Rout, C. S. Electrochemical biosensors based on Ti3C2Tx MXene: Future perspectives for on-site analysis. *Curr. Opin. Electrochem.* **2021**, 100782.

(49) Boateng, A.; Brajter-Toth, A. Nanomolar detection of p-nitrophenol via in situ generation of p-aminophenol at nanostructured microelectrodes. *Analyst* **2012**, *137*, 4531−4538.

(50) Wang, K.; Wu, C.; Wang, F.; Jiang, G. MOF-Derived CoP x Nanoparticles Embedded in Nitrogen-Doped Porous Carbon Polyhedrons for Nanomolar Sensing of p-Nitrophenol. *ACS Appl. Nano Mater.* **2018**, *1*, 5843−5853.

(51) Iqbal, A.; Hong, J.; Ko, T. Y.; Koo, C. M. Improving oxidation stability of 2D MXenes: synthesis, storage media, and conditions. *Nano Convergence* **2021**, *8*, 1−22.

(52) Giribabu, K.; Suresh, R.; Manigandan, R.; Munusamy, S.; Kumar, S. P.; Muthamizh, S.; Narayanan, V. Nanomolar determination of 4-nitrophenol based on a poly (methylene blue)-modified glassy carbon electrode. *Analyst* **2013**, *138*, 5811−5818.

(53) Zhang, R.; Liu, J.; Li, Y. MXene with great adsorption ability toward organic dye: an excellent material for constructing a ratiometric electrochemical sensing platform. *ACS sensors* **2019**, *4*, 2058−2064.

(54) Tecuapa-Flores, E. D.; Turcio-Ortega, D.; Hernandez, J. G.; Huerta-Aguilar, C. A.; Thangarasu, P. The role of keto group in cyclic ligand 1, 4, 8, 11-tetraazacyclotetradecane-5, 7-dione as strong corrosion inhibitor for carbon steel surface: Experimental and theoretical studies. *J. Mol. Struct.* **2019**, *1189*, 131−145.

(55) Cruz-Borbolla, J.; Garcia-Ochoa, E.; Narayanan, J.; Maldonado-Rivas, P.; Pandiyan, T.; Vásquez-Pérez, J. M. Electrochemical and theoretical studies of the interactions of a pyridyl-based corrosion inhibitor with iron clusters (Fe15, Fe30, Fe45, and Fe60). *J. Mol. Model.* **2017**, *23*, 1−15.

(56) Garcia-Ochoa, E.; Guzmán-Jiménez, S. J.; Hernández, J. G.; Pandiyan, T.; Vásquez-Pérez, J. M.; Cruz-Borbolla, J. Benzimidazole ligands in the corrosion inhibition for carbon steel in acid medium: DFT study of its interaction on Fe30 surface. *J. Mol. Struct.* **2016**, *1119*, 314−324.

(57) Gutiérrez, E.; Rodríguez, J. A.; Cruz-Borbolla, J.; Alvarado-Rodríguez, J. G.; Thangarasu, P. Development of a predictive model for corrosion inhibition of carbon steel by imidazole and benzimidazole derivatives. *Corros. Sci.* **2016**, *108*, 23−35.

(58) Camacho-Mendoza, R. L.; Gutiérrez-Moreno, E.; Guzmán-Percástegui, E.; Aquino-Torres, E.; Cruz-Borbolla, J.; Rodríguez-Ávila, J. A.; Alvarado-Rodríguez, J. G.; Olvera-Neria, O.; Thangarasu, P.; Medina-Franco, J. L. Density functional theory and electrochemical studies: structure−efficiency relationship on corrosion inhibition. *J. Chem. Inf. Model.* **2015**, *55*, 2391−2402.

(59) Zhang, Y.; Jiang, X.; Zhang, J.; Zhang, H.; Li, Y. Simultaneous voltammetric determination of acetaminophen and isoniazid using MXene modified screen-printed electrode. *Biosens. Bioelectron.* **2019**, *130*, 315−321.

(60) Li, S.-M.; Wang, Y.-S.; Hsiao, S.-T.; Liao, W.-H.; Lin, C.-W.; Yang, S.-Y.; Tien, H.-W.; Ma, C.-C. M.; Hu, C.-C. Fabrication of a silver nanowire-reduced graphene oxide-based electrochemical biosensor and its enhanced sensitivity in the simultaneous determination of ascorbic acid, dopamine, and uric acid. *J. Mater. Chem. C* **2015**, *3*, 9444−9453.

(61) Emmanuel, R.; Karuppiah, C.; Chen, S.-M.; Palanisamy, S.; Padmavathy, S.; Prakash, P. Green synthesis of gold nanoparticles for trace level detection of a hazardous pollutant (nitrobenzene) causing Methemoglobinaemia. *J. Hazard. Mater.* **2014**, *279*, 117−124.

(62) Madhu, R.; Karuppiah, C.; Chen, S.-M.; Veerakumar, P.; Liu, S.-B. Electrochemical detection of 4-nitrophenol based on biomass derived activated carbons. *Anal. Methods* **2014**, *6*, 5274−5280.

(63) Karuppiah, C.; Palanisamy, S.; Chen, S. M.; Emmanuel, R.; Ali, M. A.; Muthukrishnan, P.; Prakash, P.; Al-Hemaid, F. Green biosynthesis of silver nanoparticles and nanomolar detection of p-nitrophenol. *J. Solid State Electrochem.* **2014**, *18*, 1847−1854.

(64) Pontié, M.; Thouand, G.; De Nardi, F.; Tapsoba, I.; Lherbette, S. Antipassivating electrochemical process of glassy carbon electrode (GCE) dedicated to the oxidation of nitrophenol compounds. *Electroanalysis* **2011**, *23*, 1579−1584.

(65) Zhang, C. J.; Pinilla, S.; McEvoy, N.; Cullen, C. P.; Anasori, B.; Long, E.; Park, S.-H.; Seral-Ascaso, A.; Shmeliov, A.; Krishnan, D.; Morant, C.; Liu, X.; Duesberg, G. S.; Gogotsi, Y.; Nicolosi, V. Oxidation Stability of Colloidal Two-Dimensional Titanium Carbides (MXenes). *Chem. Mater.* **2017**, *29*, 4848−4856.

(66) Jiao, X. X.; Luo, H. Q.; Li, N. B. Fabrication of graphene−gold nanocomposites by electrochemical co-reduction and their electro-catalytic activity toward 4-nitrophenol oxidation. *J. Electroanal. Chem.* **2013**, *691*, 83−89.

(67) Yin, H.; Zhou, Y.; Ai, S.; Liu, X.; Zhu, L.; Lu, L. Electrochemical oxidative determination of 4-nitrophenol based on a glassy carbon electrode modified with a hydroxyapatite nanopowder. *Microchim. Acta* **2010**, *169*, 87−92.

(68) Zhang, C.; Govindaraju, S.; Giribabu, K.; Huh, Y. S.; Yun, K. AgNWs-PANI nanocomposite based electrochemical sensor for detection of 4-nitrophenol. *Sens. Actuators, B* **2017**, *252*, 616−623.

(69) Kubendhiran, S.; Sakthivel, R.; Chen, S.-M.; Mutharani, B.; Chen, T.-W. Innovative strategy based on a novel carbon-black− β-cyclodextrin nanocomposite for the simultaneous determination of the anticancer drug flutamide and the environmental pollutant 4-nitrophenol. *Anal. Chem.* **2018**, *90*, 6283−6291.